UHASSELT
KNOWLEDGE IN ACTION

Maastricht University

Faculty of Medicine and Life Sciences
School for Life Sciences
Master of Biomedical Sciences

Master's thesis

Effects of micro- and nanoplastics on an intestinal in vitro model: Investigating uptake, barrier function, cytotoxicity, and molecular stress responses

Anneleen Peeters

Thesis presented in fulfillment of the requirements for the degree of Master of Biomedical Sciences, specialization Environmental Health Sciences

SUPERVISOR :

Prof. dr. Nelly SAENEN

MENTOR :

Mevrouw Ines TEJEDA

2024
2025

Transnational University Limburg is a unique collaboration of two universities in two countries: the University of Hasselt and Maastricht University.

UHASSELT
KNOWLEDGE IN ACTION

www.uhasselt.be
Universiteit Hasselt
Campus Hasselt:
Martelarenlaan 42 | 3500 Hasselt
Campus Diepenbeek:
Agoralaan Gebouw D | 3590 Diepenbeek

UHASSELT
KNOWLEDGE IN ACTION

Maastricht University

Faculty of Medicine and Life Sciences
School for Life Sciences
Master of Biomedical Sciences

Master's thesis

Effects of micro- and nanoplastics on an intestinal in vitro model: Investigating uptake, barrier function, cytotoxicity, and molecular stress responses

Anneleen Peeters

Thesis presented in fulfillment of the requirements for the degree of Master of Biomedical Sciences, specialization Environmental Health Sciences

SUPERVISOR :

Prof. dr. Nelly SAENEN

MENTOR :

Mevrouw Ines TEJEDA

Effects of micro- and nanoplastics on an intestinal *in vitro* model: Investigating uptake, barrier function, cytotoxicity, and molecular stress responses

Anneleen Peeters[1], Ines Tejeda[2], Karen Smeets[2] and Nelly Saenen[2]

[1]Student Environment Health Sciences, Hasselt University, Diepenbeek, Belgium
[2]Zoology: Biodiversity and Toxicology research group, Centre for Environmental Sciences (CMK), Hasselt University, Campus Diepenbeek, Agoralaan Building D -3590 Diepenbeek, Belgium

The toxicity of MNPs on the intestinal barrier

To whom correspondence should be addressed: Prof. dr. Nelly Saenen, Tel: +3211268330; Email: nelly.saenen@uhasselt.be

Keywords: Micro- and nanoplastics (MNPs), Caco-2/HT29-MTX co-culture model, UV-aging, transepithelial electrical resistance (TEER), LDH cytotoxicity assay, particle uptake, confocal microscopy, gene expression analysis

ABSTRACT

Human exposure to micro- and nanoplastics (MNPs) through food and drinking water is an emerging health concern, as their small size makes them difficult to remove from the environment, allowing accumulation in the food chain. MNPs may interact with the intestinal epithelium, but data on their cellular effects remain limited, particularly under environmentally realistic conditions. In the environment, plastics undergo UV-aging, which can alter their surface properties and affect biological interactions. This study aims to assess the impact of virgin and UV-aged MNPs of different polymer types (polyamide, polyethylene terephthalate, and polyvinyl chloride), various sizes, concentrations, and exposure durations on the small intestinal epithelium using a relevant *in vitro* model. Toxicity was assessed through lactate dehydrogenase release for cytotoxicity, transepithelial electrical resistance for barrier integrity, confocal microscopy for particle uptake, and gene expression analysis targeting oxidative stress, endoplasmic reticulum stress, mitochondrial dynamics, and autophagy.

Results revealed a pattern of size- and concentration-dependent effects. Smaller particles (<1 µm) and higher concentrations (100 µg/mL) were most frequently associated with cytotoxicity, uptake, and altered stress-related gene expression. Effects of UV-aging were less consistent: while UV-aged MNPs appeared more cytotoxic in LDH assays, this was not consistently reflected in uptake or gene expression data. These findings highlight the complex interplay between particle characteristics and biological responses. This study emphasizes the importance of including environmentally relevant aged MNPs in toxicity assessments. It provides valuable insights into MNP-induced intestinal effects and supports further research and policy development to mitigate human health risks associated with plastic pollution.

INTRODUCTION

The continuous increase in plastic production, combined with the poor waste management, has led to the accumulation of plastic debris across various ecosystems, including marine, freshwater, terrestrial, and atmospheric environments (1). As larger plastic items degrade through physical, chemical, and biological processes, they break down into smaller particles known as microplastics (MPs) and nanoplastics (NPs), collectively referred to as micro- and nanoplastics (MNPs). These small plastic particles are now widely distributed throughout the environment and are recognized as emerging contaminants of concern for both ecosystems and human health (2). MNPs are categorized based on their size: MPs range from 1 µm to 5 mm, while NPs are defined as particles smaller than 1 µm (3). These particles originate from various sources. Bottom-up MNPs are intentionally manufactured at microscopic scales for use in products such as cosmetics, toothpaste, and industrial applications (4). In contrast, top-down MNPs result from the degradation of larger plastic items, including photodegradation driven

by ultraviolet (UV) radiation (1, 2, 5). Plastics consist of a wide range of polymers, such as polyamide (PA), polyvinyl chloride (PVC), polyethylene terephthalate (PET), polystyrene (PS) and polypropylene (PP), among others (2, 6). This study will focus on three specific polymer types: PA, which is widely used in textiles and carpets; PET, commonly found in beverage bottles and food packaging; and PVC, frequently used in pipes, flooring, and medical equipment (7, 8). Their widespread production and use make them major contributors to environmental plastic pollution, highlighting their relevance for this research. The environmental persistence and potential toxicity of MNPs have raised concerns among scientists, policymakers, and the public (9). Their small size allows them to be ingested by a wide range of organisms, leading to bioaccumulation and potential biomagnification through food webs (10, 11). Moreover, MNPs can act as vectors for other pollutants, such as heavy metals and persistent organic pollutants, further increasing their impact on ecosystems and human health (12).

MNPs in the environment are subject to aging processes that can significantly alter their physical and chemical characteristics (13). These aging processes are generally categorized into biotic and abiotic mechanisms (14). Biotic aging refers to the breakdown and transformation of plastics through interactions with microorganisms and their enzymatic activity (14). Abiotic aging includes photoaging (caused by sunlight, especially UV radiation), thermal degradation (due to temperature fluctuations), and mechanical aging (from wind, waves, or abrasion by particles such as sand) (13). Among these, photoaging is considered a crucial driver of environmental transformation of MNPs (15). When exposed to UV light, MNPs can undergo surface oxidation, fragmentation, and changes in surface charge and hydrophobicity (16). These transformations not only affect the environmental fate and mobility of MNPs but may also influence their interactions with biological systems (16). Interestingly, photoaging affects microplastics (MPs) and nanoplastics (NPs) to varying degrees. For instance, virgin polystyrene (PS) NPs generate more reactive oxygen species (ROS) upon light irradiation compared to PS MPs, likely due to their larger specific surface area, which offers more reaction sites and surface defects for UV absorption and radical formation (17). Smaller PS NPs also show higher reactivity during photodegradation, leading to the production of low-molecular-weight compounds such as formic acid, benzoic acid, lactic acid, and benzaldehyde (18). Importantly, factors such as the presence of ions, natural organic matter, and minerals in the surrounding matrix can accelerate photoaging by enhancing the generation of reactive species (16). As a result, UV-aged MNPs often exhibit different surface properties, sizes, and reactivities compared to virgin particles, features that may increase their potential to cause adverse biological effects (13, 16).

Since these aging processes commonly occur in the environment, the MNPs that humans are exposed to through food and water are more likely to be aged than virgin. Given that aging alters physicochemical properties, environmentally aged particles may exhibit distinct biological interactions following ingestion, making them especially relevant for toxicological assessment (19). The changes caused by aging, such as altered surface chemistry and increased reactivity, can influence how these particles interact with biological systems after ingestion, making aged MNPs particularly relevant for assessing potential health risks. Due to the small size of MNPs, they are difficult to filter out, facilitating their persistence in the environment, accumulation in ecosystems, and integration into the food chain (11). Consequently, humans are continuously exposed to MNPs through multiple pathways: ingestion, inhalation, and dermal contact (1, 20). Ingestion is considered the primary route of exposure, with MNPs detected in a wide range of consumables (21). While seafood is a well-known source of MNP exposure due to bioaccumulation in marine organisms, many other common foods also contribute (1, 22). MNPs have been detected in table salt, tap water, and bottled water. Additionally, agricultural soils have been found to contain high levels of MNPs, up to 67.5 grams or 236,000 particles per kilogram of soil (23). These particles can be taken up by crops and transferred into edible parts, meaning rice, vegetables, and fruits may also be contaminated (22). Recent estimates suggest that in Europe, shellfish consumption alone accounts for an intake of approximately 11,000 MNP particles per person per year (20). Depending on individual dietary habits, total annual intake from various food sources may range between 39,000 and 52,000 particles per person (12, 20, 24, 25). The widespread distribution of MNPs in diverse food

items reflects the continuous, daily ingestion of these particles by humans, although the associated health risks remain poorly understood (12).

The link between environmental aging and biological effects is particularly relevant to the gastrointestinal (GI) tract, the primary site of interaction for ingested MNPs (26). Within the GI tract, MNPs may compromise intestinal barrier integrity by inducing oxidative stress, local inflammation, and internal aberration, ultimately leading to increased permeability (9, 26-28). MNPs also induce cellular senescence by promoting mitochondrial dysfunction, impairing autophagy, and activating DNA damage responses, potentially leading to accelerated aging and transgenerational health risks (29). In addition, recent studies have implicated MNPs in triggering endoplasmic reticulum (ER) stress and impairing mitochondrial dynamics, processes that are closely linked to autophagy and cellular homeostasis (30). MNPs may also compromise tissue and blood barriers through mechanical disruption, contributing to chronic inflammation, genomic alterations, and possibly carcinogenic outcomes (27). Particle size plays a critical role in toxicity: larger MNPs are generally trapped in the mucus layer, potentially leading to localized inflammation, while smaller MNPs more readily penetrate the intestinal lining and enter systemic circulation, causing widespread exposure throughout the body in mammals (9, 27). These smaller particles are especially associated with oxidative stress, mitochondrial dysfunction, and pro-inflammatory responses in intestinal tissues (27). Although research is still limited, several recent studies suggest that UV-aged MNPs may exert more pronounced biological effects than their virgin counterparts. For instance, UV-aged PS nanoparticles have been shown to induce greater intestinal barrier damage compared to virgin PS, likely due to increased production of ROS, particularly hydroxyl radicals, leading to lipid peroxidation and oxidative injury (19).

To investigate the biological impacts of MNP exposure, an *in vitro* intestinal co-culture model composed of Caco-2 and HT29-MTX cells is utilized. Caco-2 cells will replicate the absorptive properties of enterocytes, exhibiting an apical brush border structure, while HT29-MTX cells will serve as a model for mucus-secreting goblet cells, the second predominant cell type within the intestinal epithelium (31-33). Together, these cell types provide a comprehensive representation of the human intestinal barrier by mimicking the gut epithelium. Compared to monocultures, co-culture systems better replicate the complex cellular architecture and physiological functions of the intestinal barrier, including mucus production, which can modulate the interaction, transport, and toxicity of MNPs (33).

Despite the growing body of research on the potential toxicity of MNPs, significant knowledge gaps remain. Most MNP toxicity studies have relied on commercially available, virgin MNPs, typically spherical and monosized particles (9). Yet, only a limited number of studies have compared how such virgin versus aged particles affect intestinal cells. By including environmentally aged MNPs, this study provides a more realistic representation of human exposure and helps to clarify how photoaging influences MNP-induced intestinal toxicity.

This study addresses this gap by comparing the effects of virgin and UV-aged MNPs on an intestinal co-culture model (Caco-2/HT29-MTX) using several toxicological endpoints, including LDH release to assess cytotoxicity, TEER measurements for barrier integrity, confocal imaging to evaluate particle uptake, and gene expression analysis focusing on oxidative stress, endoplasmic reticulum stress, mitochondrial dynamics, and autophagy. The primary objectives of this research are to determine how MNP size, polymer type, and UV-aging influence cellular uptake, oxidative stress, gene expression, and cytotoxicity. By systematically comparing these factors across different plastics, sizes, and conditions, including virgin and UV-aged states, this study aims to fill critical knowledge gaps regarding MNP toxicity. The findings will provide valuable insights into the health risks associated with MNP exposure, supporting the development of regulations to mitigate plastic pollution and protect human health. Additionally, they will contribute to the growing evidence on the health implications of MNPs, emphasizing the importance of sustainable waste management and plastic production practices to protect both human health and the environment.

EXPERIMENTAL PROCEDURES

Cell culture and maintenance – Adherent human epithelial colorectal adenocarcinoma cells (Caco-2, ATCC® HTB37TM, LGC Standards, Wesel,

Table 1 - Overview of experimental conditions. The table summarizes the plastic types, aging conditions, particle size ranges, and concentrations tested, along with the corresponding assays performed at each timepoint (6 h, 24 h, and 48 h). Assays listed in each table entry correspond to those conducted at the indicated timepoint under the respective exposure condition.

Plastic	Aging	Size	Concentration	6H	24H	48H
Polyamide (PA)	UV	<1 µm	10 (µg/mL)	TEER, LDH, gene expression	TEER, LDH, gene expression	TEER, LDH
		1–5 µm	10 (µg/mL)	TEER, LDH, gene expression	TEER, LDH, gene expression	TEER, LDH
		1–5 µm	100 (µg/mL)	TEER, LDH, gene expression	TEER, LDH, gene expression	TEER, LDH
Polyethylene terephthalate (PET)	Virgin	<1 µm	10 (µg/mL)	TEER, LDH, gene expression	TEER, LDH, gene expression	TEER, LDH
		1–5 µm	10 (µg/mL)	TEER, LDH, gene expression	TEER, LDH, gene expression	TEER, LDH
	UV	<1 µm	10 (µg/mL)	TEER, LDH, gene expression	TEER, LDH, gene expression	TEER, LDH
		1–5 µm	100 (µg/mL)	TEER, LDH, gene expression	TEER, LDH, gene expression	TEER, LDH
Polyvinyl chloride (PVC)	Virgin	<1 µm	10 (µg/mL)	TEER, LDH, gene expression	TEER, LDH, gene expression	TEER, LDH
		1–5 µm	10 (µg/mL)	TEER, LDH, gene expression	TEER, LDH, gene expression	TEER, LDH
	UV	<1 µm	10 (µg/mL)	TEER, LDH, uptake, gene expression	TEER, LDH, uptake, gene expression	TEER, LDH, uptake
		1–5 µm	10 (µg/mL)	TEER, LDH, uptake, gene expression	TEER, LDH, uptake, gene expression	TEER, LDH, uptake
		1–5 µm	100 (µg/mL)	TEER, LDH, gene expression	TEER, LDH, gene expression	TEER, LDH
Green fluorescent polyvinyl chloride (PVC)	Virgin	<1 µm	10 (µg/mL)	Uptake	Uptake	Uptake
		1–5 µm	10 (µg/mL)	Uptake	Uptake	Uptake

Germany) and adherent human epithelial colon cells (HT29-MTX-E12, ECACC 12040401, Salisbury, United Kingdom) were cultured and maintained in 75 cm² and 25 cm² cell culture flasks, respectively (Greiner, Sigma-Aldrich, Darmstadt, Germany), containing Dulbecco's Modified Eagle Medium (DMEM, Gibco, Fisher Scientific, Brussels, Belgium) supplemented with 10% heat-inactivated fetal bovine serum (FBS, Sigma-Aldrich, Darmstadt, Germany), 1% penicillin/streptomycin (Gibco, Fisher Scientific, Brussels, Belgium), and 1% nonessential amino acids (MEM-NEAA, Gibco, Fisher Scientific, Brussels, Belgium). Cells were grown in TC inserts (Sarstedt, Nümbrecht, Germany), made of polyethylene terephthalate (PET) with a pore size of 3 µm in diameter, placed in 12-well and 24-well plates, using a co-culture seeded at a 9:1 ratio of Caco-2 to HT29-MTX cells. A total of 25,000 cells were seeded per well in the 24-well plates

and 100,000 cells per well in the 12-well plates. The cells were maintained at 37°C with 5% CO_2, and the culture medium was refreshed every two to three days. To allow differentiation into an *in vitro* intestinal epithelial barrier, the co-culture was maintained under these conditions for three weeks before exposure to micro- and nanoplastics (MNPs). For the experiments, Caco-2 cells at passage numbers 30-38 were used, while HT29-MTX-E12 cells were used at passage numbers 5-10.

Exposure of the co-culture – As part of the Momentum 2.0 project, a collaborative initiative investigating the biological effects of MNPs, this study used standardized virgin and UV-aged MNPs. To ensure consistency across participating research groups, UV-aged particles were centrally prepared using UV radiation. The MNPs were derived from three commonly used plastics: polyvinyl chloride (PVC), polyethylene terephthalate (PET), and polyamide (PA). Following three weeks of differentiation, the co-culture was exposed to MNPs applied on the apical compartment of the TC inserts for 6, 24, or 48 hours. Exposures were conducted in phenol red-free Dulbecco's Modified Eagle Medium (DMEM, Gibco, Fisher Scientific, Brussels, Belgium) supplemented with 10% heat-inactivated fetal bovine serum (FBS, Sigma-Aldrich, Darmstadt, Germany). Details on the plastic types, aging conditions, concentrations, and their use across different assays are provided in Table 1.

TEER – To ensure the integrity and functionality of the co-culture, transepithelial electrical resistance (TEER) was measured using an epithelial volt-ohmmeter (Millicell® ERS-2, Merck Millipore, Burlington, Massachusetts, United States). Measurements were taken at each culture medium exchange following the manufacturer's instructions. During each culture medium change, TEER was measured in six randomly selected wells. All wells were measured for TEER both before (PRE) and after (POST) exposure. For each measurement, an insert without cells was included as a blank. TEER was then calculated by subtracting the blank and correcting for the insert's growth surface area.

LDH assay – Cell viability was assessed by measuring lactate dehydrogenase (LDH) release using the CyQUANT™ LDH Cytotoxicity Assay, following the manufacturer's instructions (Fisher Scientific, Brussels, Belgium). LDH release was quantified by measuring absorbance at 490 nm and 680 nm using a microplate reader (Fluostar Omega, BMG Labtech, Champigny-sur-Marne, France) within one hour. All values were normalized using the controls of the same plate (more details in Supplementary S1).

Semi-quantitative assessment of MNP uptake – To assess particle uptake in a semi-quantitative manner, co-cultures were exposed to fluorescently labeled particles. For virgin PVC, green-fluorescent particles were used, while PVC UV particles were stained with iDye Pink (Supplementary S2a). Following exposure, cells were fixed with 4% paraformaldehyde (PFA; Sigma-Aldrich, Darmstadt, Germany) for 15 minutes at room temperature and washed with phosphate-buffered saline (PBS; VWR®, Radnor, Pennsylvania, United States). Fixed samples were stored in PBS containing 0.1% sodium azide at 4°C until staining. Following fixation, cells were stained with DAPI at a 1:2000 dilution in PBS for 15 minutes at room temperature, and with CellMask™ Actin Tracking Stain at 1:1000 in PBS for 24 hours at 4°C with gentle shaking. Deep Red or Green Actin stain was used depending on particle color, with red fluorescence applied when particles were green, and green when particles were red. Stains were from Invitrogen (Fisher Scientific, Brussels, Belgium). Following staining, membranes were mounted apical side up using ProLong™ Gold Antifade Mountant and covered with a 24x24 mm coverslip. Slides were allowed to polymerize for 24 hours at room temperature in the dark and stored at 4°C until imaging. A more detailed description of the staining and mounting procedures is provided in Supplementary S2b. Confocal imaging was performed using a laser scanning confocal microscope (CLSM; LSM 900, Zeiss, Zaventem, Belgium) equipped with high-power diode lasers (excitation wavelengths: 405, 488, 514, and 633 nm). Mounted samples were positioned with the apical side facing downward and imaged using a 40x oil immersion water-based objective lens. Z-stack images were acquired in bidirectional scan mode using frame scan acquisition, with a z-step size of 0.15 µm to ensure high-resolution 3D imaging. The same microscope settings were applied across all samples to ensure consistency for semi-quantitative analysis. All images were adjusted using the same settings in ZEN Blue software

(v3.11) to enhance particle visibility, and substacks were manually selected based on predefined cell compartments. Using Fiji (v1.54g), the particle fluorescence channels were isolated, and maximum intensity projections were created for each substack. Particles were manually counted per region, following the image analysis workflow described in the Supplementary Figure S3a. Uptake percentage was calculated by dividing the total number of particles for the apical compartment by the total number of cells and multiplying by 100. This was also done for the microvilli compartment, resulting in the %microvilli.

Gene expression analysis – Gene expression analysis was performed using quantitative real-time polymerase chain reaction (RT-qPCR) to

Table 2 – List of selected genes with primer sequences

Gene	Name	Forward Primer (5'-3')	Reversed Primer (5'-3')
Autophagy-related genes			
ATG7	Autophagy related 7	TGAGTTGACCCAGAAGAAGCT	CCCAGCAGAGTCACCATTGT
ATG14	Autophagy related 14	CAATCGAGGAAGTAAAGACGG	TCGTCCTGAGAGGTAAGTTG
NBR1	NBR1 autophagy cargo receptor	GGTATCCATCAACAGTCAAGG	CGTTTTGCTCCTACAACTGG
Endoplasmic reticulum stress genes			
ATF4	Activating transcription factor 4	ATGACCGAAATGAGCTTCCTG	GCTGGAGAACCCATGAGGT
CHOP	DNA damage inducible transcript 3	AGAACCAGGAAACGGAAACAGA	TCTCCTTCATGCGCTGCTTT
Mitochondrial dynamics genes			
FIS1	Fission, mitochondrial 1	AGATGGACTCGTGGGCATGG	ACAGGGAAAGGACAGCGAGG
MFF	Mitochondrial fission factor	AACCCCTGGCACTGAAAACA	TGAGGGGTTGTAGGAGGTCT
MFN1	Mitofusin 1	CCTTTTACCTCAGCCTCCCA	CAGACCCAAGGATCCACACT
Oxidative stress genes			
CAT	Catalase	AGCTTAGCGTTCATCCGTGT	GCCACTAGCTTGCATTTG
GPX1	Glutathione peroxidase 1	TCCGGGACTACACCCAGATG	TCTTGGCGTTCTCCTGATGC
GPX4	Glutathione peroxidase 4	GCCTTCCCGTGTAACCAGTT	TTCATCCACTTCCACAGCGG
HMOX1	Heme oxygenase 1	CTGCTCAACATCCAGCTCTTTG	CTCCACGGGGGCAGAATCTT
PTGS2	Prostaglandin-endoperoxide synthase 2	TTGCTGGCAGGGTTGCTGGTGGTA	CATCTGCCTGCTCTGGTCAATCGAA
SLC7A11	Solute carrier family 7 member 11	CTCCAGGTTATTCTATGTTGCGTCT	CAAAGGGTGCAAAACAATAACAGC
SOD1	Superoxide dismutase 1	TGCAGGTCCTCACTTTAATCCTC	AGTCTCCAACATGCCTCTCTTC
SOD2	Superoxide dismutase 2	AGCCCAGATAGCTCTTCAGC	CCAGCAACTCCCCTTTGGG
TFRC	Transferrin receptor	GCTGGAGACTTTGGATCGGTTGG	TATACAACAGTGGGCTGGCAGAAAC
Reference genes			
GAPDH	Glyceraldehyde-3-phosphate dehydrogenase	TGTTCGTCATGGGTGTGAAC	ATGGCATGGACTGTGGTCAT
RPLP0	Ribosomal protein P0	CGTCCTCGTGGAAGTGACAT	TAGTTGGACTTCCAGGTCGC
TBP	TATA-box binding protein	CACGAACCACGGCACTGATT	TTTTCTTGCTGCCAGTCTGGAC
UBC	Ubiquitin C	CAGCCGGGATTTGGGTCG	CACGAAGATCTGCATTGTCAAGT

assess molecular stress responses (Table 2). To preserve RNA integrity, RLT lysis buffer (QIAGEN, Hilden, Germany) was freshly supplemented with 1% β-mercaptoethanol (Sigma-Aldrich, St. Louis, Missouri, United States) immediately before use. Following exposure, 50 µL of the prepared lysis buffer was added to each well to lyse the cells, and the resulting lysates were frozen at −80°C for subsequent RNA extraction. Total RNA was extracted within two weeks using phenol–chloroform extraction. RNA purity (260/280 and 260/230 absorbance ratios) and concentration (absorbance at 260 nm) were assessed with a Nanodrop spectrophotometer (ND-1000, Fisher Scientific, Brussels, Belgium). After gDNA wipeout (TURBO DNA-free™ Kit, Invitrogen, Fisher Scientific, Brussels, Belgium), RNA was reverse-transcribed into cDNA using the GoScript™ Reverse Transcription System (Promega, Madison, Wisconsin, USA) according to the manufacturer's protocol. Gene expression analysis was performed using the QuantStudio 5 RT-qPCR system (Applied Biosystems, Fisher Scientific, Brussels, Belgium) in a 384-well format. Each well contained a 7,5 µL mastermix with Fast SYBR Green PCR Master Mix (Applied Biosystems, Fisher Scientific, Brussels, Belgium), 0.3 mM forward and reverse primers, and RNAse-free water, combined with 2.5 µL of 6.0 ng/µL cDNA. The PCR program consisted of an initial denaturation at 95°C for 20 s, followed by 40 cycles of 95°C for 1 s and 60°C for 20 s. To quantify relative gene expression, the $2^{-\Delta\Delta Ct}$ method was applied, with normalization to four validated reference genes (Table 2). Four reference genes were selected using the qBase software in combination with geNorm, ensuring the stability and suitability of the chosen genes for normalization of gene expression data.

Statistical analysis – All cellular assays included three biological repeats and repeated twice in independent experiments unless stated otherwise. All statistical analyses were conducted using software R (version 4.3.3). For all the data, the normality of the distributions was first assessed using the Shapiro–Wilk test. If the assumption of normality was not met, a log transformation of the data was applied. If assumptions of normality or homogeneity of variances were violated and could not be corrected, a non-parametric test, the Kruskal–Wallis test, was applied. Post hoc comparisons were carried out using Tukey's Honest Significant Difference (HSD) test following significant Analysis of Variance (ANOVA) results, or the Dunn test with Benjamini–Hochberg correction for multiple comparisons, following significant Kruskal–Wallis tests. A p-value of less than 0.05 was considered statistically significant for all analyses. All figures were made using GraphPad unless stated otherwise.

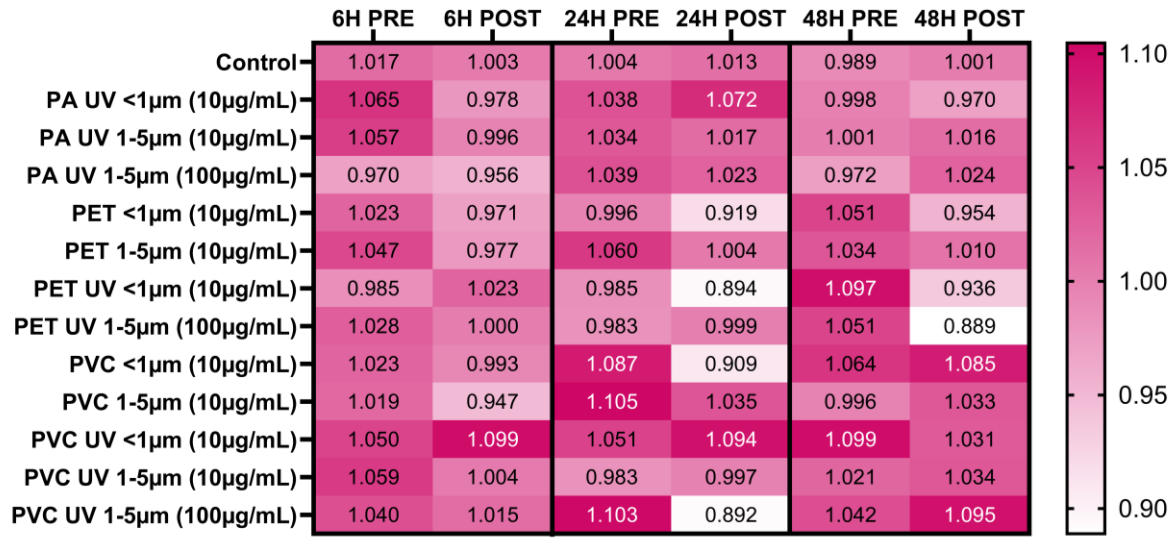

Figure 1 - Heatmap of TEER measurements in co-cultures exposed to MNPs. The heatmap displays normalized TEER values before (PRE) and after (POST) exposure for each condition and timepoint (6, 24, and 48 hours). The color gradient indicates values respect to the control (1.0). Co-cultures were treated with PA, PET, or PVC particles, either virgin or UV-aged, in two size ranges (<1 µm and 1–5 µm) and at two concentrations (10 µg/mL and 100 µg/mL). For all conditions n = 6-10, except for the controls n = 16-20. Wilcoxon signed-rank test was performed for differences between PRE- and POST-exposure values within each condition. Multiple testing correction was applied using the Benjamini-Hochberg method. No statistically differences were found.

RESULTS

TEER – Transepithelial electrical resistance (TEER) measurements were used to assess epithelial barrier integrity following exposure to micro- and nanoplastics (MNPs). No statistically significant differences were found, neither between the different exposure conditions nor between the measurements taken before and after exposure for each condition at each timepoint. This lack of significance may be attributed to the high variability in the data, which is clearly reflected in the large deviation bars and is likely due to limited statistical power caused by high inter-sample variability (Supplementary Figure S4). Overall, no consistent or clear patterns were observed across conditions (Figure 1). However, a decrease in TEER values from before (PRE) to after (POST) exposure was observed under specific conditions, including PET UV <1 µm (10 µg/mL, 48 h), PET UV 1–5 µm (100 µg/mL, 48 h), and PVC UV 1–5 µm (100 µg/mL, 24 h) (Figure 1).

LDH assay – Cytotoxicity was assessed using the lactate dehydrogenase (LDH) release assay, which measures membrane integrity by quantifying LDH released from damaged cells. Similar to the TEER results, LDH data showed a broad range of responses across conditions. The normalized LDH values demonstrated considerable variability, which limited the ability to detect statistically significant differences (Figure 2). However, at 48 hours, exposure to

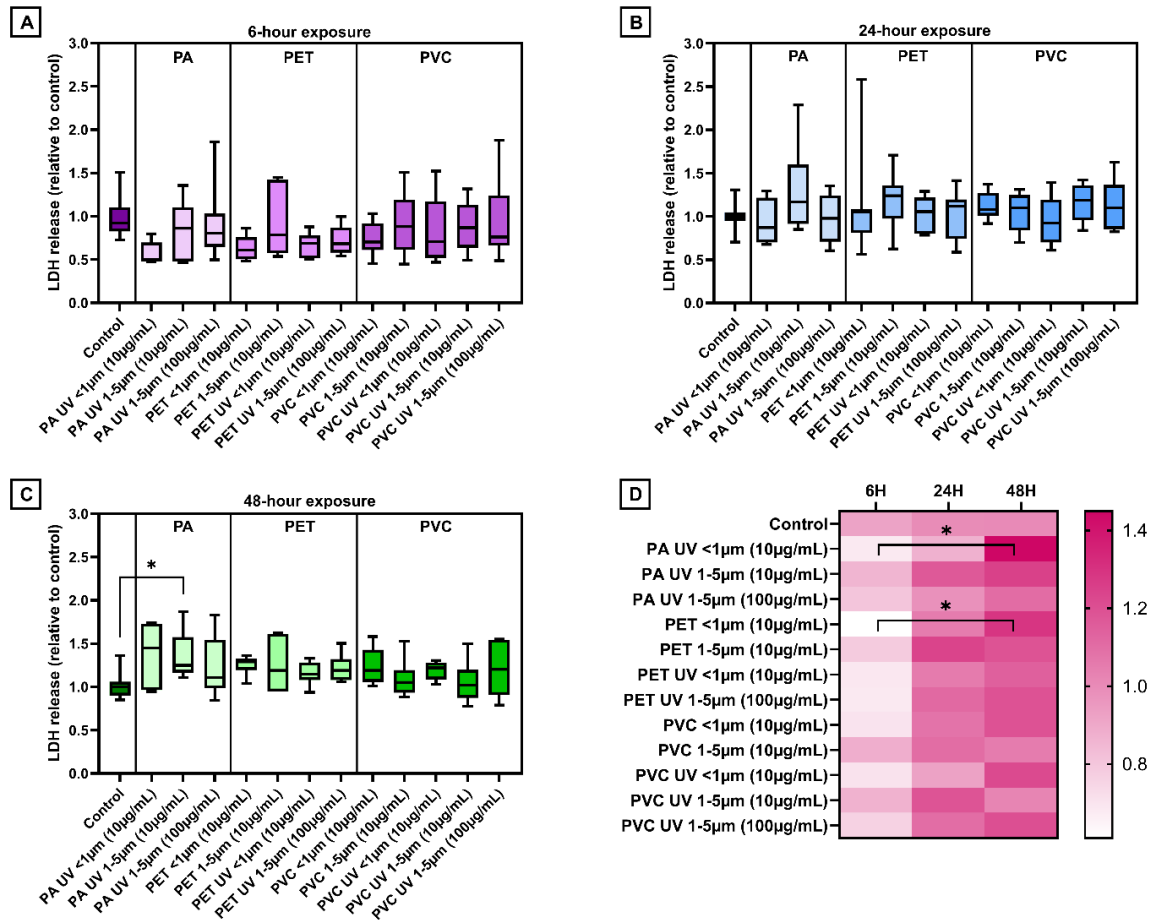

Figure 2 – LDH release from the co-culture exposed to MNPs. Co-cultures were treated with PA, PET, or PVC particles, either virgin or UV-aged, in two size ranges (<1 µm and 1–5 µm) and at two concentrations (10 µg/mL and 100 µg/mL). Untreated cultures served as controls. **(A)** The box-and-whisker plots shows LDH release normalized to control after 6 hours. **(B)** The box-and-whisker plots shows LDH release normalized to control after 24 hour exposure. **(C)** The box-and-whisker plots shows LDH release normalized to control after 48 h. For all the box-and-whisker plots, data represent median, interquartile range, and full data range (minimum–maximum whiskers) for each condition and timepoint. **(D)** Heatmap of LDH release in co-cultures exposed to MNPs over time. The color gradient indicates values respect to the control (1.0). For all conditions n = 6-10, except for the controls n = 16-20. Data were log-transformed following assessment of normality. One-way ANOVA followed by Tukey's HSD post hoc test was used to compare conditions at each timepoint. Asterisks above brackets indicate statistically significant differences ($p < 0.05$).

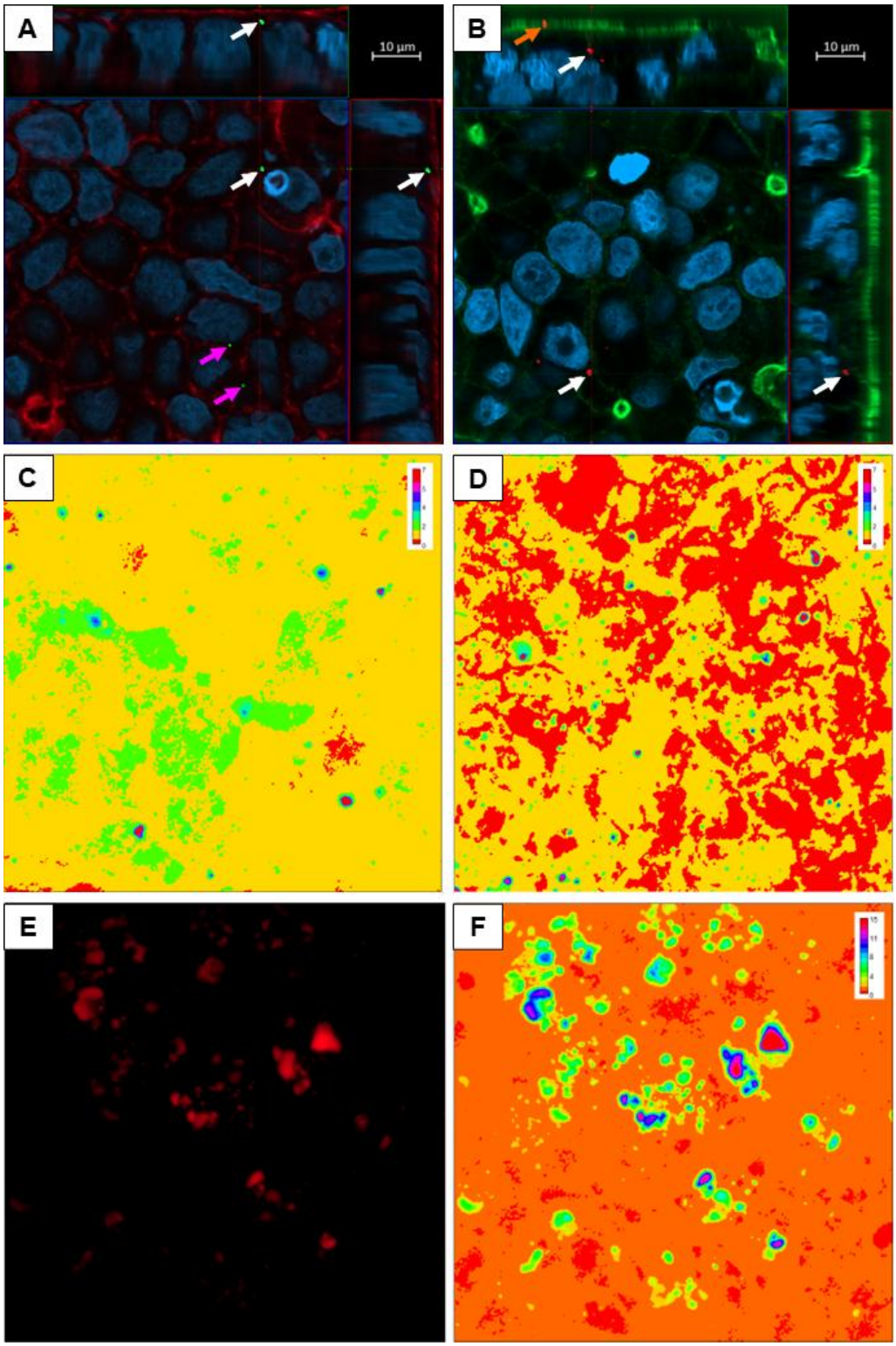

Figure 3 – Visualization and quantification of particle localization in co-cultures exposed to PVC or PVC UV, either particles <1 µm or 1-5 µm using a concentration of 10 µg/ml. **(A)** Confocal microscopy image of co-culture exposed to PVC <1 µm for 6 hours showing nuclei (blue); cell membranes (red), and particles (green). The white arrows show the same particle across the different orthogonal planes. Orthogonal views (top and right) provide spatial context for particle localization in the apical–basal axis. The pink arrows point out two other particles that were taken up. **(B)** Confocal microscopy image of co-culture exposed to PVC UV 1–5 µm for 24 hours showing nuclei (blue), cell membranes (green), and particles (red). The white arrows show the same particle across the different orthogonal planes. The orange arrow points out another particle, stuck between the microvilli. **(C–F)** Fiji analyses of the particle channel. C and D are LUT-transformed images showing particle intensity (C: microvilli region, PVC UV 1–5 µm, 6 h; D: apical cell region, PVC <1 µm, 24 h). Particle quantification was based on the two to three highest LUT colors on the calibration bar. E shows the original red-channel image of the nucleus region (PVC UV 1–5 µm, 6 h), used as the basis for the LUT transformation shown in F.

PA UV 1–5 µm (10 µg/mL) resulted in a significant increase in LDH release compared to the control ($p = 0.0383$) (Figure 2C). In contrast to the TEER measurements, LDH release exhibited a clearer overall trend of increasing cytotoxicity over time across most exposure conditions, whereas LDH levels in control samples remained relatively stable (Figure 2D). When comparing timepoints within the same condition, two significant increases in LDH release were observed: PA UV <1 µm (10 µg/mL) ($p = 0.0003$) and PET <1 µm (10 µg/mL) ($p = 0.0019$) both showed significantly elevated LDH levels at 48 hours compared to 6 hour exposure. Although these were the only statistically significant changes over time, a similar upward trend was visually apparent in most conditions, with stronger effects observed for particles <1 µm.

Development of semi-quantitative image analysis method for MNP quantification – To enable semi-quantitative analysis of particle uptake, an image analysis method was developed (Supplementary S3b). For the PVC and PVC UV samples, alternative settings were applied during confocal imaging, as these particles were visible in a different channel, which also included a different

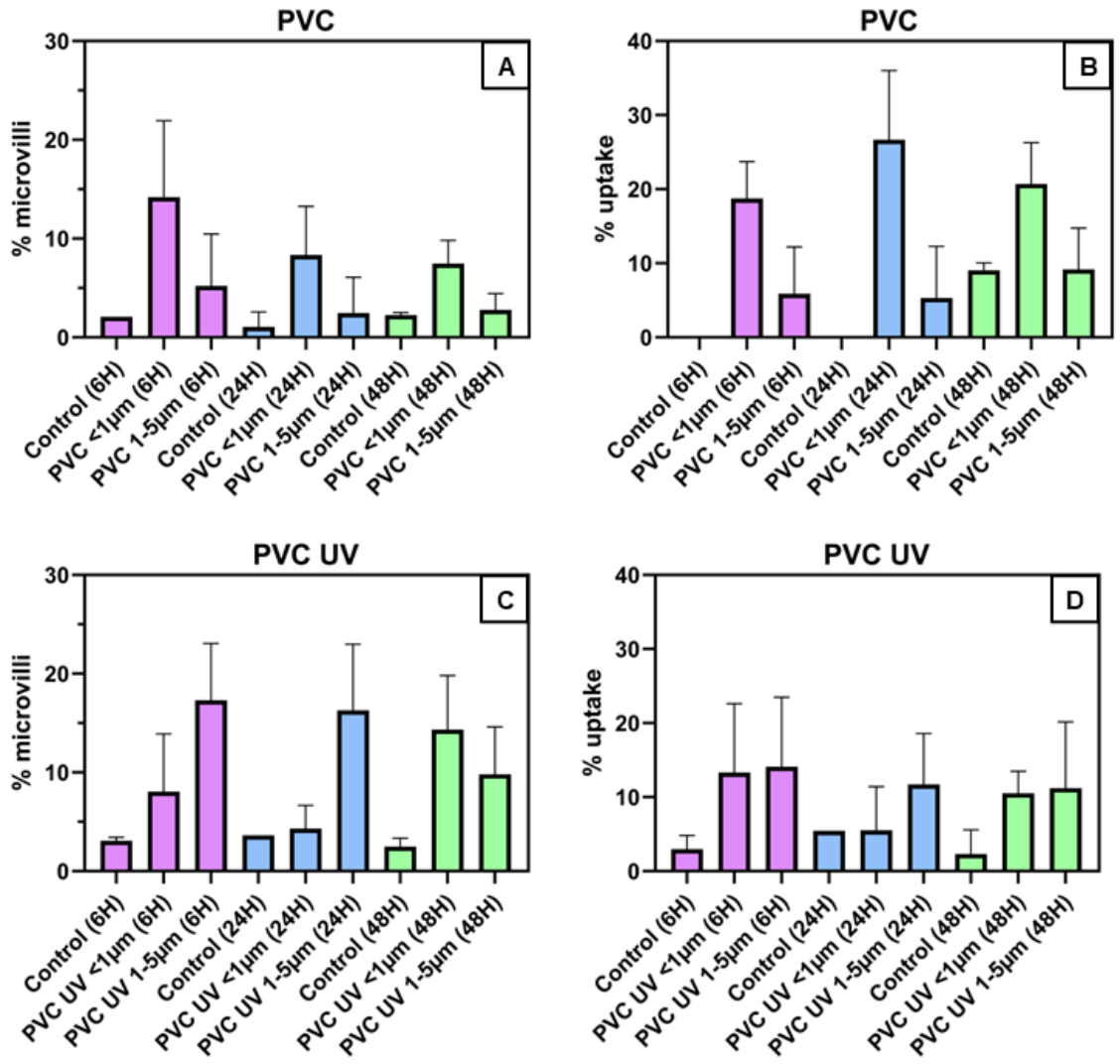

Figure 4 – Semi-quantitative analysis of particle uptake in different cellular compartments. **(A)** Quantification of virgin PVC in the microvilli region. **(B)** Quantification of virgin PVC in the apical region of the cell. **(C)** Quantification of UV-aged PVC in the microvilli region. **(D)** Quantification of UV-aged PVC in the apical region of the cell. Co-cultures were exposed to virgin or UV-aged PVC particles in two size ranges (<1 µm and 1–5 µm) at a concentration of 10 µg/mL for 6, 24, or 48 hours. Untreated cultures served as controls. Data are presented as bar plots (mean ± standard deviation). The y-axis shows the percentage of particles of a region, calculated as: (number of particles in the compartment of interest / number of cells per image) × 100. The x-axis represents the different conditions. For all conditions n = 2-6, except for the controls n = 1-2. Statistical analysis was performed using a Kruskal–Wallis test followed by Dunn's post hoc test.

actin staining (Deep Red versus Green) (Figure 3A and 3B). Several steps in the analysis process require particular attention, as they may introduce variability or reduce reproducibility. Despite using identical settings for each image, differences in background fluorescence were observed between confocal images. As part of the method, the start and end z-slices corresponding to each cellular compartment were manually identified and recorded in an Excel file. This step was essential for making substacks of the different regions in the cell. In the final step, the particles and cells were also manually counted, which may contribute to additional variability. The method proved to be effective for quantifying particles in both the microvilli (%microvilli) and apical regions (%uptake) of the cells (Figure 3A and 3B). In contrast, the nuclear region displayed elevated background fluorescence, which was already apparent in the original 8-bit images and became more pronounced when using the LUT spectrum for analysis (Figure 3E and 3F). This interference prevented accurate particle identification in the nuclear compartment. Therefore, quantification was restricted to the microvilli and apical regions (Figure 3C and 3D). In control samples, a consistent background signal was observed in both the microvilli and apical compartments, with an average of approximately 3%.

Semi-quantitative analysis of PVC and PVC UV uptake – Confocal imaging showed high variability, resulting in no statistically significant differences between conditions. However, trends in particle uptake (for the apical region) were evident. PVC <1 µm particles showed the highest uptake, peaking at ~27% particles after 24 hours, while larger particles (1–5 µm) were taken up less, especially at earlier timepoints (Figure 4B). Uptake for both sizes declined by 48 hours (Figure 4B). In contrast, uptake of PVC UV particles was lower and more variable, with no clear time-dependent pattern observed across size ranges (Figure 4D). For PVC particles, a higher percentage of particles was observed between the microvilli at 6 hours compared to 48 hours, particularly for <1 µm particles (Figure 4A). So, this proportion declined over time. For PVC UV particles, 1–5 µm particles consistently showed greater microvilli association across all timepoints, with a slight decrease at 48 hours (Figure 4C).

Gene expression – Gene expression changes following MNP exposure were assessed for markers of oxidative stress, ER stress, mitochondrial dynamics, and autophagy at 6, and 24 hours. Most genes did not exhibit statistically or biologically meaningful differences compared to the control. Gene expression changes are generally considered biologically relevant when they exceeded a twofold change. Although some genes surpassed this threshold (Figure 6), these changes were often not statistically significant. This was largely due to biological variability and the loss of several samples, as certain exposure conditions had limited replicates, reducing the statistical power to detect significant effects. The only significant finding compared to the control was for the 6-hour exposure increased for the gene *CHOP*: PVC UV 1–5 µm (100 µg/mL, 6 h) with a p-value of 0.0087 (Figure 5). For the 24-hour timepoint, a few genes (*ATG7* and *MFN1*) showed significance in the non-parametric test, but after correction, nothing remained statistically significant. Based on polymer type, it appears that PET and PVC exposures lead to more consistent gene expression changes compared to PA, which generally resulted in weaker or inconsistent responses (Figure 6).

For autophagy, the only gene with a consistent trend was *ATG7*, which showed a general increase in expression at 24 hours, especially under exposure to smaller particles or 1–5 µm particles at the higher concentration of 100 µg/mL. *ATG14* and *NBR1* showed no consistent pattern and fluctuated without a clear time- or dose-dependent response (Figure 6).

In the context of ER stress, *ATF4* showed no consistent expression changes across polymers or timepoints. *CHOP*, on the other hand, showed the most notable and biologically relevant changes. Primarily at 6 hours, exposure to smaller particles or 1–5 µm particles at higher concentrations led to increased expression levels, particularly under PET <1 µm (10 µg/mL), PVC <1 µm (10 µg/mL), PET UV 1–5 µm (100 µg/mL), and PVC UV 1–5 µm (100 µg/mL). These four conditions exceeded the twofold change threshold, with the PVC UV condition reaching statistical significance (Figure 5 and 6).

For mitochondrial dynamics, *FIS1* expression was inconsistent and fluctuated across conditions and timepoints, showing no reproducible pattern. *MFF* exhibited an increase only for PET, particularly at 6 hours and for both particle sizes, both virgin and UV-aged, with several of these conditions exceeding the twofold change

threshold. *MFN1* showed a general increasing trend across many exposure conditions and both timepoints, but only PVC UV 1–5 µm (100 µg/mL, 6 h) exceeded the twofold threshold, making it the only condition with a biologically relevant response for this gene (Figure 6).
Oxidative stress responses were limited, with most genes such as *CAT*, *GPX4*, *SOD1* and *SOD2* showing stable or inconsistent expression. *GPX1* displayed a subtle increasing trend in expression, with four conditions exceeding the twofold threshold: PA UV <1 µm (10 µg/mL, 24 h); PET 1–5 µm (10 µg/mL, 24 h); PVC <1 µm (10 µg/mL, 6 h); and PVC UV 1–5 µm (10 µg/mL, 6 h). Interestingly, *HMOX1* showed a consistent downregulation at 6 hours for nearly all polymer types and conditions, with the strongest effects seen in PET and PVC, regardless of UV treatment. Most values return closer to baseline by 24 h. *PTGS2* displayed sporadic increases, primarily for PET and PVC under exposure to smaller particles or higher concentrations, with levels returning closer to baseline by 24 hours.

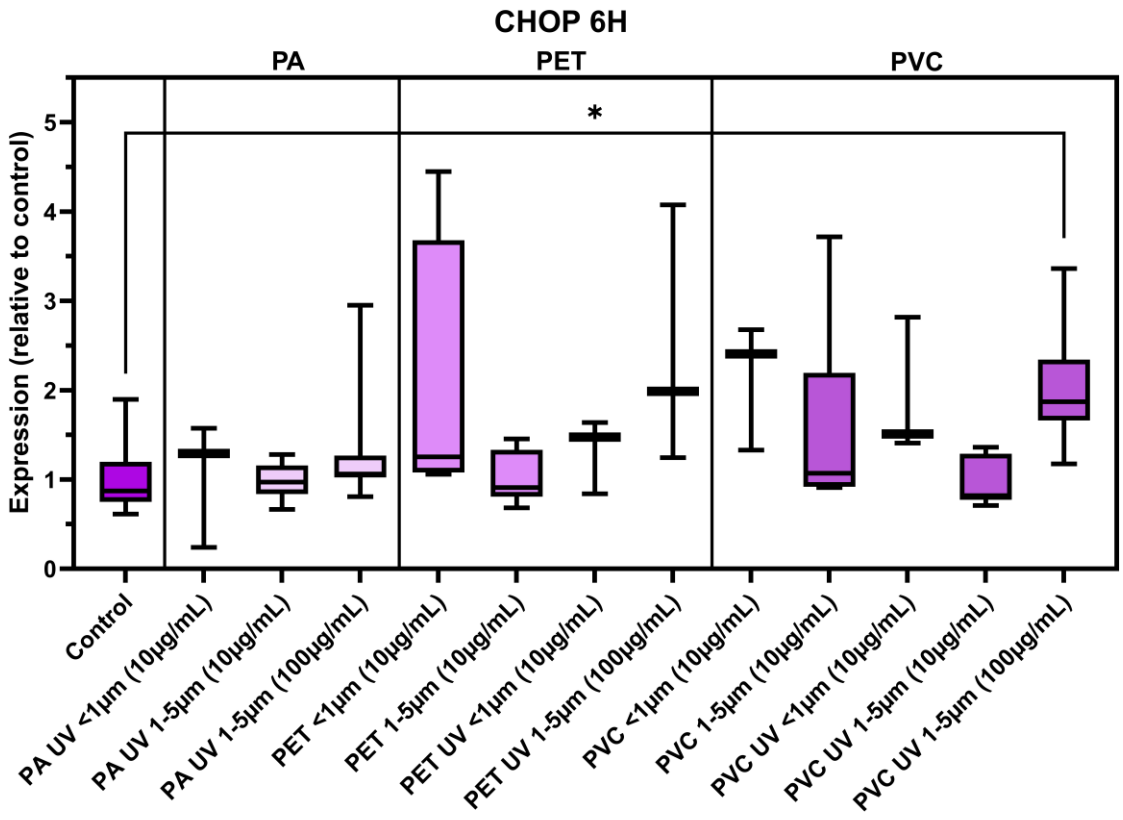

Figure 5 – *CHOP* expression levels after 6 hours following exposure to various MNPs. The box-and-whisker plots represent *CHOP* expression levels relative to control. Co-cultures were treated with PA, PET, or PVC particles, either virgin or UV-aged, in two size ranges (<1 µm and 1–5 µm) and at two concentrations (10 µg/mL and 100 µg/mL). Data represent median, interquartile range, and full data range (minimum–maximum whiskers) for each condition. For all conditions n = 3-8, except for the control n = 9. Following a significant Kruskal-Wallis test, a Dunn's test many-to-one post hoc test was performed under different conditions against the control group ($p < 0.05$).

		POLYAMIDE (PA)									
		VIRGIN				UV					
		<1 µm		1-5 µm		<1 µm		1-5 µm			
		10 µg/ml		10 µg/ml		10 µg/ml		10 µg/ml	100 µg/ml	10 µg/ml	100 µg/ml
	Gene	6H	24H	6H	24H	6H	24H	6H		24H	
Autophagy	ATG7					0,359	1,325	0,993	1,045	1,347	1,045
	ATG14					0,657	0,687	1,216	0,959	1,116	1,138
	NBR1					0,989	1,103	0,974	0,911	1,057	1,215
ER stress	ATF4					0,642	0,928	0,942	1,046	0,969	0,932
	CHOP					1,034	0,916	0,983	1,301	0,833	1,198
Mitochondrial dynamics	FIS					0,591	1,211	0,714	0,851	1,014	0,909
	MFF					0,575	1,018	1,329	0,876	0,959	0,976
	MFN1					0,989	0,711	1,176	1,332	1,321	1,350
Oxidative stress/ antioxidants	CAT					0,837	0,860	0,940	0,826	1,041	1,125
	GPX1					1,075	3,272	0,874	1,168	1,175	1,197
	GPX4					0,789	1,026	0,982	1,008	1,070	1,017
	HMOX1					0,328	1,017	0,521	0,638	0,875	0,933
	PTGS2					0,643	0,988	1,101	0,714	0,915	0,751
	SLC7A11					0,589	1,002	1,073	1,056	0,685	0,958
	SOD1					1,204	0,903	0,926	1,014	0,992	0,949
	SOD2					0,691	0,955	1,066	0,909	0,972	1,041
	TFRC					0,783	0,910	1,009	0,870	1,031	1,085
		POLYETHYLENE TEREPHTHALATE (PET)									
Autophagy	ATG7	1,039	1,878	0,975	0,941	0,641	1,869		1,147		1,744
	ATG14	1,161	1,321	0,946	1,089	1,140	1,012		1,232		0,944
	NBR1	1,314	1,113	0,739	1,107	1,222	1,072		1,316		1,092
ER stress	ATF4	1,272	0,992	0,913	1,113	1,081	1,088		1,321		0,976
	CHOP	2,004	0,736	1,019	1,769	1,317	0,765		2,436		1,354
Mitochondrial dynamics	FIS	1,141	0,971	0,645	1,668	1,369	1,107		1,369		0,899
	MFF	3,713	1,118	0,809	0,924	0,511	4,662		1,574		0,826
	MFN1	1,344	1,289	0,977	1,170	1,584	0,604		1,702		1,015
Oxidative stress/ antioxidants	CAT	1,096	0,934	0,694	0,875	1,283	1,075		1,078		0,859
	GPX1	1,761	0,949	0,870	4,271	1,411	0,651		1,660		1,277
	GPX4	1,000	0,844	0,983	0,830	1,362	1,136		1,013		0,767
	HMOX1	0,610	0,881	0,653	0,742	0,330	0,737		0,505		1,259
	PTGS2	1,284	1,455	0,842	1,226	1,399	1,002		1,649		1,029
	SLC7A11	1,162	1,023	0,880	0,750	1,153	1,325		0,614		0,995
	SOD1	1,225	0,936	0,968	1,231	1,414	0,723		1,391		0,982
	SOD2	1,304	1,331	0,790	0,897	1,106	1,107		1,149		1,042
	TFRC	1,196	0,996	0,763	0,742	1,386	1,209		1,031		0,859
		POLYVINYL CHLORIDE (PVC)									
Autophagy	ATG7	0,954	1,314	1,147	0,995	0,784	1,638	0,956	1,295	0,993	1,065
	ATG14	1,145	0,954	1,071	1,067	0,847	0,853	0,758	1,049	1,273	1,020
	NBR1	1,599	0,945	0,940	1,215	1,062	1,376	0,722	0,753	1,068	0,998
ER stress	ATF4	1,147	0,796	0,917	1,028	1,166	1,171	0,890	1,329	0,908	0,972
	CHOP	2,137	1,125	1,562	1,926	1,911	1,014	0,973	2,031*	1,257	1,786
Mitochondrial dynamics	FIS	1,140	0,688	0,752	1,135	0,902	1,859	0,581	0,987	0,977	0,820
	MFF	1,164	0,976	1,030	1,214	0,996	0,952	0,730	1,224	0,973	0,952
	MFN1	1,174	0,985	1,178	1,521	1,159	0,802	0,992	7,393	1,475	1,097
Oxidative stress/ antioxidants	CAT	0,953	0,769	0,877	0,868	0,894	1,630	0,698	1,036	1,075	0,838
	GPX1	2,083	0,981	1,363	1,444	1,534	1,054	2,568	1,341	1,230	1,150
	GPX4	0,991	0,914	0,792	0,934	1,091	1,124	0,872	0,826	0,999	0,954
	HMOX1	0,839	0,801	0,633	1,085	0,416	0,952	0,741	0,808	1,153	0,859
	PTGS2	1,757	1,120	1,018	1,132	0,950	0,833	1,138	3,119	1,023	1,084
	SLC7A11	0,735	1,327	0,799	0,816	0,930	1,230	0,729	1,104	0,882	0,867
	SOD1	1,284	0,768	1,072	1,012	1,438	1,043	0,843	0,822	1,087	0,960
	SOD2	1,145	1,023	0,947	1,007	0,762	1,358	0,735	0,814	1,095	0,808
	TFRC	1,441	0,990	0,767	1,027	0,744	1,138	0,821	0,870	1,133	1,116

Figure 6 – Heatmap of average relative gene expression per condition after 6 h and 24 h exposure to MNPs. The heatmap displays the group average of relative gene expression for each gene and condition, compared to their respective control. Expression levels were calculated using the $2^{-\Delta\Delta Ct}$ method, with *GAPDH*, *RPLP0*, *TBP*, and *UBC* as reference genes. The genes analyzed are involved in autophagy, ER stress, mitochondrial function, and oxidative stress. Exposure conditions differ by polymer type (PET, PVC, PA), particle size (<1 µm or 1–5 µm), UV status (virgin or UV-aged), and concentration (10 or 100 µg/mL). The color gradient ranges from red to blue, where red indicates a decrease and blue indicates an increase in relative gene expression compared to control. For 6 h exposure, n = 6-8 for all conditions, except for <1 µm and 10 µg/mL PA UV, PET, PET UV, PVC, and PVC UV, and for PET UV (1-5 µm and 100 µg/mL), where n = 3-4. For 24 h exposure, n = 6-9 for all conditions, except for <1 µm and 10 µg/mL PVC, PVC UV, and PET UV, where n = 4-5. For the 6 h control, n = 9, and for the 24 h control, n = 18. An asterisk (*) indicates statistically significant differences from control ($p < 0.05$), while underlined values indicate biologically relevant changes, defined as exceeding a twofold change in expression. This figure presents only group averages and does not reflect variability.

DISCUSSION

This study aimed to investigate the potential toxicological effects of micro- and nanoplastics (MNPs), both virgin and UV-aged, on a human intestinal *in vitro* co-culture model using Caco-2 and HT29-MTX cells. The primary aim was to assess how MNP characteristics (size, polymer type, and UV-aging) influenced epithelial barrier function, cytotoxicity, uptake, and gene expression. The MNPs used were heterogeneous in size, reflecting realistic environmental conditions where MNPs exist as mixed-size particles rather than uniform ones. Since environmental MNPs are often aged by ultraviolet (UV) radiation, resulting in altered surface properties, it was hypothesized that UV-aged MNPs would exert more pronounced effects on intestinal barrier function, cytotoxicity, particle uptake, and gene expression compared to virgin MNPs. Additionally, nanoscale particles (<1 µm) were expected to be more readily taken up by intestinal cells and potentially cause greater damage than larger micro-sized particles, due to their increased surface area and cellular interactions. Previous studies have often focused on virgin, monodisperse MNPs and non-human models, which do not fully represent real-world exposure or human physiology. There is a notable gap in the literature regarding the effects of environmentally aged MNPs, particularly in human-relevant intestinal models. Furthermore, limited attention has been given to the combined effects of particle size and surface aging on cellular responses. By addressing these gaps, the present study provides new insights into the intestinal responses to environmentally relevant MNPs, contributing to a more realistic toxicological understanding of human MNP exposure.

Transepithelial electrical resistance (TEER), lactate dehydrogenase (LDH), and confocal imaging are complementary assays that together provide a multifaceted understanding of the toxicological effects of MNPs on intestinal epithelial cells. TEER measurements assess the integrity of the epithelial barrier by measuring resistance across the cell monolayer. A decrease in TEER suggests disruption of tight junctions and impaired barrier function. LDH assays complement this by detecting cytoplasmic enzyme release into the medium, which indicates membrane damage and general cytotoxicity. Confocal imaging of particle uptake provides visual confirmation of whether MNPs enter the cells, helping to link internalization with functional changes. Gene expression analysis offers molecular-level insight into cellular responses, such as oxidative stress, endoplasmic reticulum (ER) stress, or autophagy. When combined, these assays allow for a comprehensive assessment of the toxicological effects of MNPs, from physical barrier damage to intracellular stress pathways.

While overall TEER trends were inconsistent, a slight time-dependent decrease in TEER was observed following exposure to PET and PVC, particularly at the 24- and 48-hour exposure, suggesting potential barrier disruption with prolonged exposure. However, these changes did not reach significance. This limited response may be explained by the relatively short exposure durations and the concentrations used (100 µg/mL), as literature has reported significant TEER reductions predominantly at longer exposures (e.g., 72 hours) and higher concentrations (up to 1000 µg/mL) (34, 35). Moreover, the variability may have masked subtle effects. Although TEER is a well-established method for evaluating tight junction integrity in epithelial cell culture models, it is known to be highly sensitive to a wide range of factors (36). Overall, the results indicate that, under the tested conditions, MNP exposure did not induce consistent or pronounced impairment of epithelial barrier integrity up to 48 hours.

In contrast to the TEER data, LDH assay revealed more consistent indications of cytotoxicity. A general increase in LDH release was observed over time and was more pronounced for UV-aged PA and PET nanoparticles (<1 µm), suggesting that smaller and aged particles induce greater membrane damage. These findings align with prior studies reporting enhanced toxicity of UV-aged MNPs. For example, Yu et al. (2022) demonstrated increased cytotoxicity of UV-aged polystyrene (PS) microparticles in Caco-2 cells, attributed to reactive oxygen species (ROS) overproduction, although effects were more pronounced at higher concentrations (500 µg/mL) (37). Similarly, increased LDH release after 24-hour exposure to UV-aged versus virgin PS was reported by another study at 150 µg/mL (38). Particle size also plays a key role in cytotoxicity: Wang et al. (2024) and Cui et al. (2023) demonstrated that smaller PS particles induced stronger cytotoxic effects than larger ones,

particularly at concentrations above 400 µg/mL (39, 40). This indicates that membrane damage is mostly induced by smaller MNPs and is likely to increase with longer exposure times and higher concentrations. Although most of these studies used polystyrene, their results help explain the effects seen here. In this study, only a few conditions showed statistically significant effects, but the overall trend of increased LDH levels at 48 hours supports the idea that UV-aged and nanoscale MNPs can increase cytotoxic stress in intestinal cells.

This study demonstrated that the uptake of MNPs by intestinal epithelial cells is influenced by particle size, and exposure duration. Specifically, PVC particles smaller than 1 µm showed the highest internalization, with uptake at the apical part of the cell reaching ~27% particles after 24 hours, followed by a decline at 48 hours. This decline at 48 hours may indicate that the particles undergo transcellular transport toward the basal side and are subsequently released, potentially entering the systemic circulation and distributing throughout the body (41). This is supported by studies reporting the presence of MNPs in human feces, colonic tissues, placenta, and even blood (1, 42, 43). In contrast, larger particles (1–5 µm) showed reduced uptake at earlier timepoints. These observations are in line with previous studies showing size- and time-dependent uptake, where smaller particles are more efficiently internalized by intestinal cells (34, 44, 45). Nanoparticles are known to cross epithelial barriers more efficiently due to their greater surface-to-volume ratio, and enhanced diffusion capacity (41). Smaller particles, particularly those in the submicron and nanometer range, show increased uptake and transport through intestinal cells compared to larger microplastics (44, 46). For PVC UV, there was not such a clear trend as seen for virgin PVC. Fewer PVC UV particles were observed between the microvilli or at the apical side of the cells. It should be noted that during the staining procedure, some adhered or loosely attached particles may have been washed off prior to confocal imaging, which could lead to an underestimation of total particle presence at the cell surface (45). These findings support the hypothesis regarding size- and time-dependent uptake, though the effect of UV-aging on uptake was less clear.

Gene expression analysis revealed a dynamic and condition-specific cellular response to MNP exposure, particularly involving pathways related to ER stress, autophagy, mitochondrial dynamics, and oxidative stress. While most genes did not exhibit statistically or biologically significant changes compared to controls, some notable trends emerged under specific conditions. One of the most prominent findings was the upregulation of *CHOP* (*DDIT3*), a key marker of ER stress. *CHOP* is a well-characterized transcription factor that promotes apoptosis during prolonged or severe ER stress by regulating the expression of both anti- and pro-apoptotic genes (47). In this study, *CHOP* expression was elevated at the 6-hour timepoint following exposure to smaller particles (<1 µm) and to 1–5 µm particles at the highest tested concentration (100 µg/mL), suggesting that early ER stress may be triggered by MNP exposure. These findings are consistent with previous studies reporting *CHOP* upregulation in intestinal cells exposed to nanoplastics or other particulate stressors (48). However, *CHOP* expression returned to baseline by 24 hours, indicating a transient ER stress response or the activation of adaptive mechanisms, such as the unfolded protein response (UPR), which help restore ER homeostasis and prevent apoptosis under moderate stress conditions (49, 50). Following the early ER stress response, a delayed upregulation of *ATG7* was observed at the 24-hour timepoint, particularly under similar exposure conditions that induced *CHOP* expression. *ATG7* is a critical component of the autophagy machinery, required for autophagosome formation and the degradation of damaged cellular components (50). PS NPs have been found to induce ER stress-mediated autophagy markers (51). Its increased expression suggests that autophagy may be activated as a secondary response, potentially to mitigate ER stress or remove damaged organelles and proteins (50). In addition to ER stress and autophagy, genes involved in mitochondrial dynamics were examined, including *MFN1* (mitofusin 1) and *MFF* (mitochondrial fission factor). These genes regulate mitochondrial fusion and fission, respectively, and are often modulated in response to cellular stress or damage (51). In this study, *MFN1* expression exceeded a twofold increase only for PVC UV 1–5 µm (100 µg/mL, 6 h), while *MFF* showed biologically relevant increases for PET <1 µm and PET UV <1 µm. These changes may reflect early mitochondrial stress or compensatory mechanisms aimed at

preserving mitochondrial function and morphology (52).
Oxidative stress responses were limited, with most genes such as *CAT*, *GPX4*, *SOD1* and *SOD2* showing stable or inconsistent expression. However, *GPX1* showed a subtle upward trend in multiple PVC and PET exposures. *HMOX1* consistently showed transient downregulation at 6 hours for most conditions, returning to baseline by 24 hours. This suggests a loss of the protective function of *HMOX1*, an important enzymatic component of the antioxidant defense system, potentially leading to increased free radical accumulation and oxidative damage (53).
Overall, when changes in gene expression were observed, they were most pronounced for the smaller particles (<1 µm) or for 1–5 µm at the highest concentration. No clear differences were observed between UV-aged and virgin particles. However, changes were typically subtle or transient, and no consistent differences were found between virgin and UV-aged particles in gene-level responses.

Taken together, the results of TEER, LDH, confocal imaging, and gene expression analysis reveal a pattern of size- and concentration-dependent effects of MNPs on intestinal epithelial cells. Across the assays, smaller particles (<1 µm) and higher concentrations (100 µg/mL) were most frequently associated with cellular responses, including increased cytotoxicity, particle uptake, and molecular stress signaling. In contrast, the effects of UV-aging were less consistent across endpoints. While the LDH assay suggested enhanced cytotoxicity for UV-aged particles, this trend was not uniformly observed in uptake or gene expression data.

A notable observation across all assays was the substantial variability between replicates and conditions. This heterogeneity can be attributed to several factors. First, the heterogeneous nature of the MNP mixtures, which likely comprise a broad distribution of particle sizes, shapes, and surface chemistries, can lead to varying and inconsistent results. Second, inconsistencies in MNP dispersion and sedimentation may result in uneven particle distribution and exposure at the cellular level. Third, batch-to-batch differences in cell differentiation and mucus layer thickness, particularly in co-culture models like Caco-2/HT29-MTX, can influence barrier integrity and particle uptake (54). Fourth, the complex physicochemical properties of environmentally relevant MNPs, such as heterogeneous size and surface characteristics, can affect their interactions with biological systems. Additionally, although standardized cell culture protocols were followed, manual cell counting (e.g., with a hemocytometer) inherently involves user-dependent variability, which can lead to slight discrepancies in seeding density and influence downstream outcomes such as proliferation and treatment sensitivity. These complexities, in combination with moderate exposure durations and lower environmentally relevant concentrations, may underlie the subtle and variable results observed. To reduce this variability in future studies, increasing the number of replicates is recommended to improve statistical power. Moreover, implementing quality checks for MNP dispersion and routinely validating mucus production in HT29-MTX cells could enhance consistency and data reliability. Together, these factors likely account for the substantial variability observed across all assays, highlighting the need for targeted measures to enhance reproducibility and data reliability in future studies.
In addition, TEER measurements, widely used to assess barrier integrity, introduced an additional layer of variability. In this study, TEER was measured using an epithelial volt-ohmmeter, a device whose readings are highly sensitive to electrode positioning (36). Precise and consistent placement of the electrodes is essential to avoid disturbing the cell layer and to ensure reproducibility (36). Moreover, temperature fluctuations during measurements can substantially impact TEER values, thereby complicating comparisons across experiments (36, 55). Finally, culture time, passage number, and seeding conditions also influence TEER measurements (56). For instance, inaccurate cell counting due to human perception error or cell clumping may lead to deviations from the intended Caco-2:HT29-MTX ratio (57). This is particularly important as immortalized cell lines such as HT29-MTX cells (goblet-type) have the potential to overgrow compared to Caco-2 cells when seeded in high proportions (36). Such imbalances can lead to altered barrier properties and TEER values, given the differential tight junction expression and mucus production characteristics of the two cell types (36).

Certainly, there are several strengths to highlight in this study. This study utilized a co-culture intestinal model (Caco-2/HT29-MTX), which

more closely mimics the *in vivo* gut environment compared to monocultures. Additionally, it focused on environmentally relevant UV-aged MNPs, increasing the ecological relevance of the findings. Assessing barrier integrity (TEER), cytotoxicity (LDH), particle uptake (imaging), and gene expression provided a comprehensive evaluation of MNP effects across different biological levels. Several limitations must be acknowledged. First, these human cancer-derived cell lines have several limitations. In particular, they tend to exhibit much higher TEER values (1600–2500 Ω·cm²) compared to those reported for the intestines *in vivo* (50–100 Ω·cm²) (34). Additionally, the mucus layer secreted by HT29-MTX-E12 cells is only 3–5 µm thick, whereas the mucus layer in the human small intestine ranges from 450–900 µm (35). These differences limit the physiological relevance of the model and make it more difficult to draw definitive conclusions about *in vivo* barrier responses. Second, although the MNPs were heterogeneous in size, reflecting environmental conditions, this complexity contributed to high sample variability, reducing statistical power and limiting the ability to draw strong conclusions. Third, the study did not simulate gastrointestinal aging processes that occur during ingestion, which could alter the physicochemical properties and biological interactions of MNPs. Fourth, the LDH assay is a widely used, cost-effective, and accessible method, relying on colorimetric detection via standard spectrophotometers (58). However, a known limitation is its relatively low sensitivity compared to other cytotoxicity assays (e.g., MTT), making it less suited for detecting subtle changes upon MNP exposure (58). Finally, confocal imaging for particle uptake requires further optimization because high background noise in the nuclear region of the cells prevented accurate assessment of whether particles penetrated beyond the apical cell layer.

Future research should focus on increasing the number of replicates to reduce sample variability and improve statistical robustness. Incorporating more complex and environmentally realistic aging processes, including simulation of gastrointestinal digestion, would enhance the ecological relevance of the results. Studies investigating chronic and repeated exposures are needed to better understand the long-term health effects of MNP ingestion. Improvements in imaging techniques with higher resolution and reduced background noise are essential for accurately assessing particle uptake and localization within intestinal cells. Furthermore, using more advanced *in vitro* models such as a triculture system including immune cells could provide valuable insights into the immune response and the overall impact of heterogeneous MNP mixtures on intestinal health.

CONCLUSION

This study aimed to investigate how micro- and nanoplastics (MNPs) of varying sizes, polymer types, and UV-aging states affect intestinal epithelial responses in a human-relevant *in vitro* co-culture model of Caco-2 and HT29-MTX cells. By integrating environmentally realistic MNP mixtures, including UV-aged particles and heterogeneous size distributions, this research provides a more ecologically relevant understanding of human MNP exposure compared to previous studies relying on virgin, monodisperse particles.

Confocal imaging demonstrated that smaller MNPs were more readily taken up by cells, particularly PVC particles <1 µm, supporting the hypothesis of size-dependent uptake. This uptake may contribute to the cytotoxic effects observed in the LDH assay, where UV-aged nanoparticles of PA and PET induced greater membrane damage than their larger counterparts. TEER measurements showed subtle, non-significant decreases in barrier integrity over time, though the overall disruption was limited, possibly due to short exposure durations and variability. Gene expression analysis further highlighted early cellular stress responses primarily triggered by smaller particles or high-concentration exposures, including transient ER stress (*CHOP*), autophagy activation (*ATG7*), and mild mitochondrial or oxidative stress signaling. Collectively, the findings underscore the complexity of MNP interactions with human intestinal cells and point to the necessity for higher-resolution techniques and refined *in vitro* models to improve reproducibility and translational relevance. Further exploration of gene regulatory responses and intracellular fate of MNPs will be crucial for fully elucidating the mechanisms driving MNP-induced intestinal effects and drawing strong conclusions.

REFERENCES

This text was supported by GenAI.

1. Yang X, Man YB, Wong MH, Owen RB, Chow KL. Environmental health impacts of microplastics exposure on structural organization levels in the human body. Sci Total Environ. 2022;825:154025.
2. Rubio-Armendáriz C, Alejandro-Vega S, Paz-Montelongo S, Gutiérrez-Fernández Á J, Carrascosa-Iruzubieta CJ, Hardisson-de la Torre A. Microplastics as Emerging Food Contaminants: A Challenge for Food Safety. Int J Environ Res Public Health. 2022;19(3).
3. Ko K, Lee J, Baumann P, Kim J, Chung H. Analysis of micro(nano)plastics based on automated data interpretation and modeling: A review. NanoImpact. 2024;34:100509.
4. Song J, Wang C, Li G. Defining Primary and Secondary Microplastics: A Connotation Analysis. ACS ES&T Water. 2024;4(6):2330-2.
5. Saenen ND, Witters MS, Hantoro I, Tejeda I, Ethirajan A, Van Belleghem F, et al. Polystyrene Microplastics of Varying Sizes and Shapes Induce Distinct Redox and Mitochondrial Stress Responses in a Caco-2 Monolayer. Antioxidants. 2023;12(3):739.
6. He B, Liu A, Ayoko G, Egodawatta P, Wijesiri B, Goonetilleke A. Microplastics as Emerging Pollutants in Urban Waterways. Environmental Risks Posed by Microplastics in Urban Waterways. Singapore: Springer Nature Singapore; 2023. p. 1-11.
7. Berry KLE, Hall N, Critchell K, Chan K, Bennett B, Mortimer M, et al. Plastics. In: Reichelt-Brushett A, editor. Marine Pollution – Monitoring, Management and Mitigation. Cham: Springer Nature Switzerland; 2023. p. 207-28.
8. Chavez-Linares P, Hoppe S, Chevalot I. Recycling and Degradation Pathways of Synthetic Textile Fibers such as Polyamide and Elastane. Global Challenges. 2025;9(4):2400163.
9. Yang Z, DeLoid GM, Zarbl H, Baw J, Demokritou P. Micro- and nanoplastics (MNPs) and their potential toxicological outcomes: State of science, knowledge gaps and research needs. NanoImpact. 2023;32:100481.
10. Liu W, Liao H, Wei M, Junaid M, Chen G, Wang J. Biological uptake, distribution and toxicity of micro(nano)plastics in the aquatic biota: A special emphasis on size-dependent impacts. TrAC Trends in Analytical Chemistry. 2024;170:117477.
11. Habumugisha T, Zhang Z, Uwizewe C, Yan C, Ndayishimiye JC, Rehman A, et al. Toxicological review of micro- and nano-plastics in aquatic environments: Risks to ecosystems, food web dynamics and human health. Ecotoxicology and Environmental Safety. 2024;278:116426.
12. Rahman A, Sarkar A, Yadav OP, Achari G, Slobodnik J. Potential human health risks due to environmental exposure to nano- and microplastics and knowledge gaps: A scoping review. Science of The Total Environment. 2021;757:143872.
13. Li H, Bai L, Liang S, Chen X, Gu X, Wang C, et al. The wheel of time: The environmental dance of aged micro- and nanoplastics and their biological resonance. Eco Environ Health. 2025;4(1):100138.
14. Binda G, Kalčíková G, Allan IJ, Hurley R, Rødland E, Spanu D, et al. Microplastic aging processes: Environmental relevance and analytical implications. TrAC Trends in Analytical Chemistry. 2024;172:117566.
15. Junaid M, Hamid N, Liu S, Abbas Z, Imran M, Haider MR, et al. Interactive impacts of photoaged micro(nano)plastics and co-occurring chemicals in the environment. Science of The Total Environment. 2024;927:172213.
16. Xu Y, Ou Q, van der Hoek JP, Liu G, Lompe KM. Photo-oxidation of Micro- and Nanoplastics: Physical, Chemical, and Biological Effects in Environments. Environmental Science & Technology. 2024;58(2):991-1009.
17. Duan J, Li Y, Gao J, Cao R, Shang E, Zhang W. ROS-mediated photoaging pathways of nano- and micro-plastic particles under UV irradiation. Water Research. 2022;216:118320.
18. Duan J, Bolan N, Li Y, Ding S, Atugoda T, Vithanage M, et al. Weathering of microplastics and interaction with other coexisting constituents in terrestrial and aquatic environments. Water Research. 2021;196:117011.
19. Jia T, Cai J, He S, Mao Z, Zhang X, Geng A, et al. UV-aged polystyrene nanoplastics aggravate intestinal barrier damage by overproduction of ROS. Environmental Toxicology and Pharmacology. 2024;108:104448.
20. Li Y, Tao L, Wang Q, Wang F, Li G, Song M. Potential Health Impact of

Microplastics: A Review of Environmental Distribution, Human Exposure, and Toxic Effects. Environment & Health. 2023;1(4):249-57.
21. Prata JC, da Costa JP, Lopes I, Duarte AC, Rocha-Santos T. Environmental exposure to microplastics: An overview on possible human health effects. Science of The Total Environment. 2020;702:134455.
22. Ramsperger AFRM, Bergamaschi E, Panizzolo M, Fenoglio I, Barbero F, Peters R, et al. Nano- and microplastics: a comprehensive review on their exposure routes, translocation, and fate in humans. NanoImpact. 2023;29:100441.
23. Zhu L, Xie C, Chen L, Dai X, Zhou Y, Pan H, et al. Transport of microplastics in the body and interaction with biological barriers, and controlling of microplastics pollution. Ecotoxicology and Environmental Safety. 2023;255:114818.
24. Sun A, Wang W-X. Human Exposure to Microplastics and Its Associated Health Risks. Environment & Health. 2023;1(3):139-49.
25. Cox KD, Covernton GA, Davies HL, Dower JF, Juanes F, Dudas SE. Human Consumption of Microplastics. Environ Sci Technol. 2019;53(12):7068-74.
26. Bora SS, Gogoi R, Sharma MR, Anshu, Borah MP, Deka P, et al. Microplastics and human health: unveiling the gut microbiome disruption and chronic disease risks. Front Cell Infect Microbiol. 2024;14:1492759.
27. Dennis J, Arulraj D, Mistri TK. Unseen toxins: Exploring the human health consequences of micro and nanoplastics. Toxicol Rep. 2025;14:101955.
28. Meng X, Zheng X, Mai W, Gao J, Fan Y, Fu J, et al. Micro- and nanoplastics differ in particle-mucus interactions: The sight on rheological properties, barrier dysfunction and microbiota dysbiosis. Journal of Hazardous Materials. 2025;492:138130.
29. Mahmud F, Sarker DB, Jocelyn JA, Sang Q-XA. Molecular and Cellular Effects of Microplastics and Nanoplastics: Focus on Inflammation and Senescence. Cells. 2024;13(21):1788.
30. Liu N, Zhang B, Lin N. Review on the role of autophagy in the toxicity of nanoparticles and the signaling pathways involved. Chemico-Biological Interactions. 2025;406:111356.
31. Costa J, Ahluwalia A. Advances and Current Challenges in Intestinal in vitro Model Engineering: A Digest. Frontiers in Bioengineering and Biotechnology. 2019;7.
32. Lea T. Caco-2 Cell Line. In: Verhoeckx K, Cotter P, López-Expósito I, Kleiveland C, Lea T, Mackie A, et al., editors. The Impact of Food Bioactives on Health: in vitro and ex vivo models. Cham (CH): Springer
Copyright 2015, The Author(s). 2015. p. 103-11.
33. Béduneau A, Tempesta C, Fimbel S, Pellequer Y, Jannin V, Demarne F, et al. A tunable Caco-2/HT29-MTX co-culture model mimicking variable permeabilities of the human intestine obtained by an original seeding procedure. Eur J Pharm Biopharm. 2014;87(2):290-8.
34. Chen Y, Williams AM, Gordon EB, Rudolph SE, Longo BN, Li G, et al. Biological effects of polystyrene micro- and nano-plastics on human intestinal organoid-derived epithelial tissue models without and with M cells. Nanomedicine. 2023;50:102680.
35. Choi H, Kaneko S, Suzuki Y, Inamura K, Nishikawa M, Sakai Y. Size-Dependent Internalization of Microplastics and Nanoplastics Using In Vitro Model of the Human Intestine—Contribution of Each Cell in the Tri-Culture Models. Nanomaterials. 2024;14(17):1435.
36. Srinivasan B, Kolli AR, Esch MB, Abaci HE, Shuler ML, Hickman JJ. TEER Measurement Techniques for In Vitro Barrier Model Systems. SLAS Technology. 2015;20(2):107-26.
37. Yu X, Lang M, Huang D, Yang C, Ouyang Z, Guo X. Photo-transformation of microplastics and its toxicity to Caco-2 cells. Science of The Total Environment. 2022;806:150954.
38. Völkl M, Jérôme V, Weig A, Jasinski J, Meides N, Strohriegl P, et al. Pristine and artificially-aged polystyrene microplastic particles differ in regard to cellular response. Journal of Hazardous Materials. 2022;435:128955.
39. Wang X, Yang Z, Ren X-M, Zhang Z, He H, Pan X. Assessment of the cytotoxicity micro- and nano-plastic on human intestinal Caco-2 cells and the protective effects of catechin. Environmental Science: Processes & Impacts. 2024;26(12):2166-76.
40. Cui M, He Q, Wang Z, Yu Y, Gao H, Liu Z, et al. Mucin2 regulated by Ho1/p38/IL-10 axis plays a protective role in polystyrene nanoplastics-mediated intestinal toxicity. Environmental Pollution. 2023;330:121808.

41. Zheng Y, Luo S, Xu M, He Q, Xie J, Wu J, et al. Transepithelial transport of nanoparticles in oral drug delivery: From the perspective of surface and holistic property modulation. Acta Pharmaceutica Sinica B. 2024;14(9):3876-900.
42. Fournier E, Leveque M, Ruiz P, Ratel J, Durif C, Chalancon S, et al. Microplastics: What happens in the human digestive tract? First evidences in adults using in vitro gut models. Journal of Hazardous Materials. 2023;442:130010.
43. Zurub RE, Cariaco Y, Wade MG, Bainbridge SA. Microplastics exposure: implications for human fertility, pregnancy and child health. Frontiers in Endocrinology. 2024;Volume 14 - 2023.
44. Paul MB, Fahrenson C, Givelet L, Herrmann T, Loeschner K, Böhmert L, et al. Beyond microplastics - investigation on health impacts of submicron and nanoplastic particles after oral uptake in vitro. Microplastics and Nanoplastics. 2022;2(1):16.
45. Elfers K, Benz P, Burmester M, Hein S, Hansen K, Sieg H, et al. Effect of nano- and micro-polystyrene particles on small intestinal epithelial functions and enteric neuronal activity in vitro. Microplastics and Nanoplastics. 2025;5(1):3.
46. Stock V, Böhmert L, Coban G, Tyra G, Vollbrecht M-L, Voss L, et al. Microplastics and nanoplastics: Size, surface and dispersant – What causes the effect? Toxicology in Vitro. 2022;80:105314.
47. Ni R, Cao T, Ji X, Peng A, Zhang Z, Fan G-C, et al. DNA damage-inducible transcript 3 positively regulates RIPK1-mediated necroptosis. Cell Death & Differentiation. 2025;32(2):306-19.
48. Lai H, Liu X, Qu M. Nanoplastics and Human Health: Hazard Identification and Biointerface. Nanomaterials (Basel). 2022;12(8).
49. Beaupere C, Labunskyy VM. (Un)folding mechanisms of adaptation to ER stress: lessons from aneuploidy. Current Genetics. 2019;65(2):467-71.
50. Liu K, Zhao C, Adajar RC, DeZwaan-McCabe D, Rutkowski DT. A beneficial adaptive role for CHOP in driving cell fate selection during ER stress. EMBO Rep. 2024;25(1):228-53.
51. Chen Q, Ruan D, Shi J, Du D, Bian C. The multifaceted roles of natural products in mitochondrial dysfunction. Frontiers in Pharmacology. 2023;Volume 14 - 2023.
52. Dal Yöntem F, Aydoğan Ahbab M. Mitochondria as a target of micro- and nanoplastic toxicity. Cambridge Prisms: Plastics. 2024;2:e6.
53. Poss KD, Tonegawa S. Reduced stress defense in heme oxygenase 1-deficient cells. Proc Natl Acad Sci U S A. 1997;94(20):10925-30.
54. Jones CF, Grainger DW. In vitro assessments of nanomaterial toxicity. Adv Drug Deliv Rev. 2009;61(6):438-56.
55. Blume LF, Denker M, Gieseler F, Kunze T. Temperature corrected transepithelial electrical resistance (TEER) measurement to quantify rapid changes in paracellular permeability. Pharmazie. 2010;65(1):19-24.
56. Chen X-M, Elisia I, Kitts DD. Defining conditions for the co-culture of Caco-2 and HT29-MTX cells using Taguchi design. Journal of Pharmacological and Toxicological Methods. 2010;61(3):334-42.
57. Vembadi A, Menachery A, Qasaimeh MA. Cell Cytometry: Review and Perspective on Biotechnological Advances. Front Bioeng Biotechnol. 2019;7:147.
58. Lewis MA, Patil K, Ettayebi K, Estes MK, Atmar RL, Ramani S. Divergent responses of human intestinal organoid monolayers using commercial in vitro cytotoxicity assays. PLOS ONE. 2024;19(6):e0304526.

Acknowledgements – I would like to express my appreciation to Prof. dr. Nelly Saenen for her invaluable guidance, support, and involvement throughout my senior internship. I am grateful to Ines Tejeda, my daily supervisor, for her mentorship and insights, who has greatly contributed to my research progress. I also would like to thank Myrthe De Puydt for her help in the lab. A warm thank you to my friends and fellow interns, Reja Trippaers and Lisa Reynders, for their help with experiments, data analysis, and for making the lab a fun and motivating environment. Finally, I would like to thank my parents, friends and family for their support, encouragement, and belief in me throughout this journey.

Author contributions – KS, NS and IT conceived and designed the research. NS, IT and AP performed experiments and data analysis. AP wrote the paper. All authors carefully edited the manuscript.

SUPPLEMENTARY

S1: Calculations/normalization LDH

To account for background interference, absorbance at 680 nm was subtracted from the 490 nm value for each sample. The average absorbance of blank wells was then subtracted from these corrected values. Unexposed control wells were included to establish baseline LDH levels. LDH release was normalized per plate to the average of the untreated control wells using the formula:

Normalized LDH release = $\frac{Sample}{Average\ of\ controls}$.

A normalized value close to one indicated minimal cytotoxicity, while deviations from one reflected altered LDH release relative to the control.

S2: ***Semi-quantitative assessment of MNP uptake***

S2a: Staining of PVC UV Particles with iDye Poly Pink – A 100 mg/mL iDye Poly Pink stock solution was prepared by dissolving iDye Poly Pink powder (Jacquard, IDYE-456, Healdsburg, CA, USA) in Milli-Q water, followed by thorough vortexing to ensure complete dissolution. For PVC UV (1–5 µm) particles, the particle stock was prepared at 10 mg/mL by diluting a 20 mg/mL suspension in sterile Milli-Q water. iDye Poly Pink was added to a final dye concentration of 0.5 mg/mL. The mixture was incubated in the dark for 3 hours at 60°C in an Eppendorf tube tightly sealed with Parafilm to prevent evaporation. Following incubation, the remaining volume was checked, and the sample was diluted with Milli-Q water to a final particle concentration of 2 mg/mL. For PVC UV (<1 µm) particles, the initial stock concentration was 1.1 mg/mL. This was diluted to 0.55 mg/mL in sterile Milli-Q water, and iDye Poly Pink was added to achieve a final dye concentration of 0.25 mg/mL. The staining suspension was also incubated in the dark for 3 hours at 60°C in a sealed Eppendorf tube wrapped with Parafilm. After incubation, the remaining volume was inspected for potential evaporation, and the sample was diluted to a final particle concentration of 0.275 mg/mL with sterile Milli-Q water.

S2b: Staining and mounting procedure of the microscopic slides - To investigate the uptake of micro- and nanoplastics (MNPs) following exposure, actin filaments and nuclei were stained. After exposure, 12-well plates were fixed with 4% paraformaldehyde (PFA; Sigma-Aldrich, Darmstadt, Germany) for 15 minutes at room temperature (RT), followed by three washes with phosphate-buffered saline (PBS; VWR®, Radnor, Pennsylvania, United States) to remove residual fixative. After fixative removal, cells were stored in PBS containing 0.1% sodium azide at 4°C until staining. Prior to staining, the membrane of each insert was carefully excised. Samples were stained with CellMask™ Deep Red Actin Tracking Stain or CellMask™ Green Actin Tracking Stain (Invitrogen, Fisher Scientific, Brussels, Belgium) at a 1:1000 dilution in phosphate-buffered saline (PBS, VWR®, Radnor, Pennsylvania, United States) and incubated for 24 hours at 4°C with gentle agitation at 150 rpm, using a microplate shaker (VWR®, Radnor, Pennsylvania, United States). Cells exposed to green fluorescent MNPs were stained with Actin Deep Red, while cells exposed to red fluorescent MNPs were stained with Actin Green. Following incubation, samples were washed three times with PBS for 5 minutes each. Nuclear staining was then performed using 4′,6-diamidino-2-phenylindole (DAPI, Invitrogen, Fisher Scientific, Brussels, Belgium) at a 1:2000 dilution in PBS for 15 minutes at room temperature, followed by three additional 5-minute washes with PBS. After staining, membranes were placed apical side up onto glass microscope slides, and mounted with three drops of ProLong™ Gold Antifade Mountant (Invitrogen, Fisher Scientific, Brussels, Belgium). A 24x24 mm coverslip was gently positioned on top, and the slide was inverted onto a piece of tissue paper. Light pressure was applied to the sides of the coverslip. Slides were left to polymerize in the dark at room temperature for 24 hours and were subsequently stored at 4°C in a light-protected box until further image acquisition and analysis.

S3: Confocal imaging and analysis

S3a: Flowchart

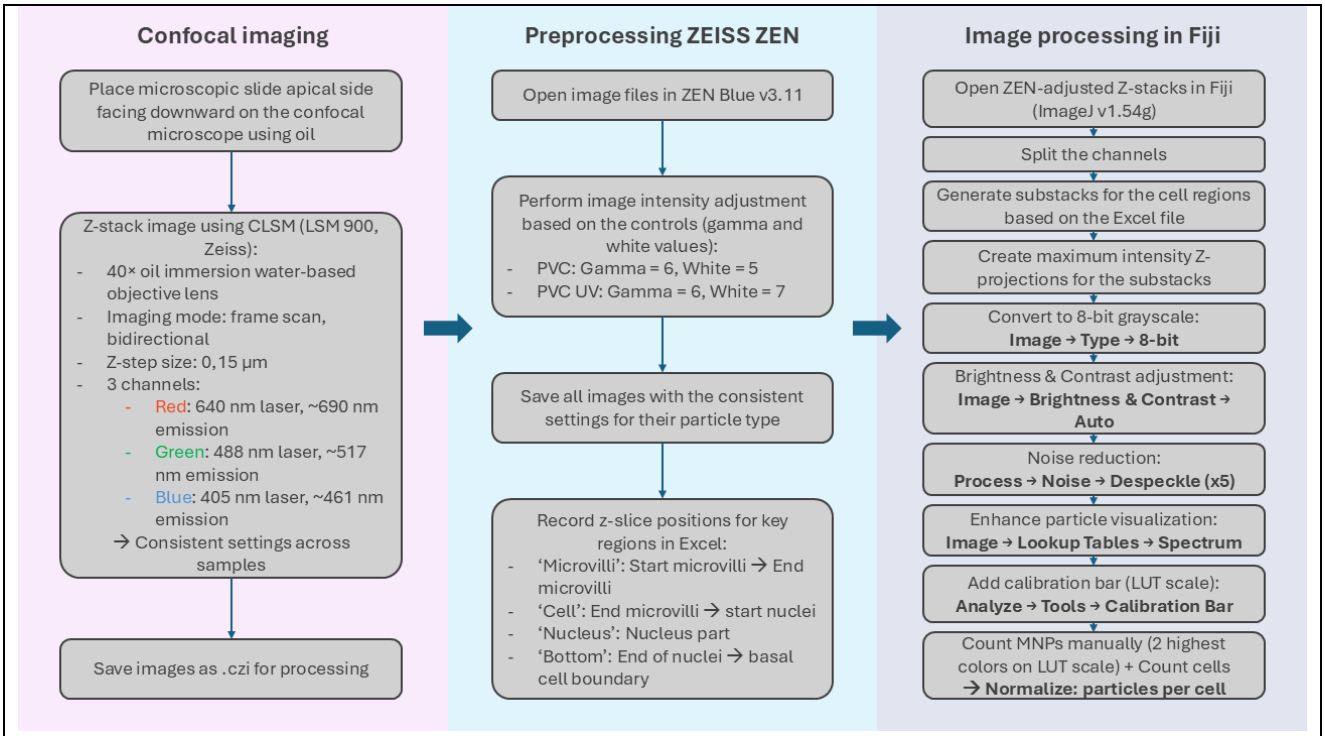

Figure S3a – Flowchart – Confocal imaging and analysis

S3b: Semi-quantitative image analysis method for MNP quantification - The following method was developed for this purpose. Following confocal imaging, all images were opened in ZEN Blue software (v3.11, Zeiss, Zaventem, Belgium) for post-processing and standardization. Gamma and white levels of the particle fluorescence channel were manually adjusted in ZEN Blue to enhance signal visualization, based on control samples. This adjustment was applied uniformly across all samples for consistency in comparative analysis (for PVC particles, gamma = 6 and white = 5; for PVC UV particles, gamma = 6 and white = 7). An Excel spreadsheet was maintained to record the z-slices corresponding to key cellular regions (e.g., microvilli, apical surface to nucleus, nucleus, basal membrane).

Saved image stacks were imported into Fiji version 1.54g (ImageJ, National Institute of Health, Bethesda, Maryland, United States). Individual fluorescence channels were separated using the "Split Channels" function with autoscaling disabled. Using the annotated z-slice ranges from the Excel file, substacks for defined cell regions were generated. Maximum intensity projections were created for each substack. Projections were converted to 8-bit format, followed by automatic brightness and contrast adjustment with the minimum brightness manually set to zero. Noise reduction was performed by applying the "Despeckle" filter five times consecutively. The "Spectrum LUT" was applied to enhance particle visualization. A calibration bar was added for fluorescence intensity reference. MNPs were manually counted corresponding to the two highest intensity colors in the LUT scale. Cells were manually counted per image to determine the number of cells present.

S4: TEER measurements for all exposure durations

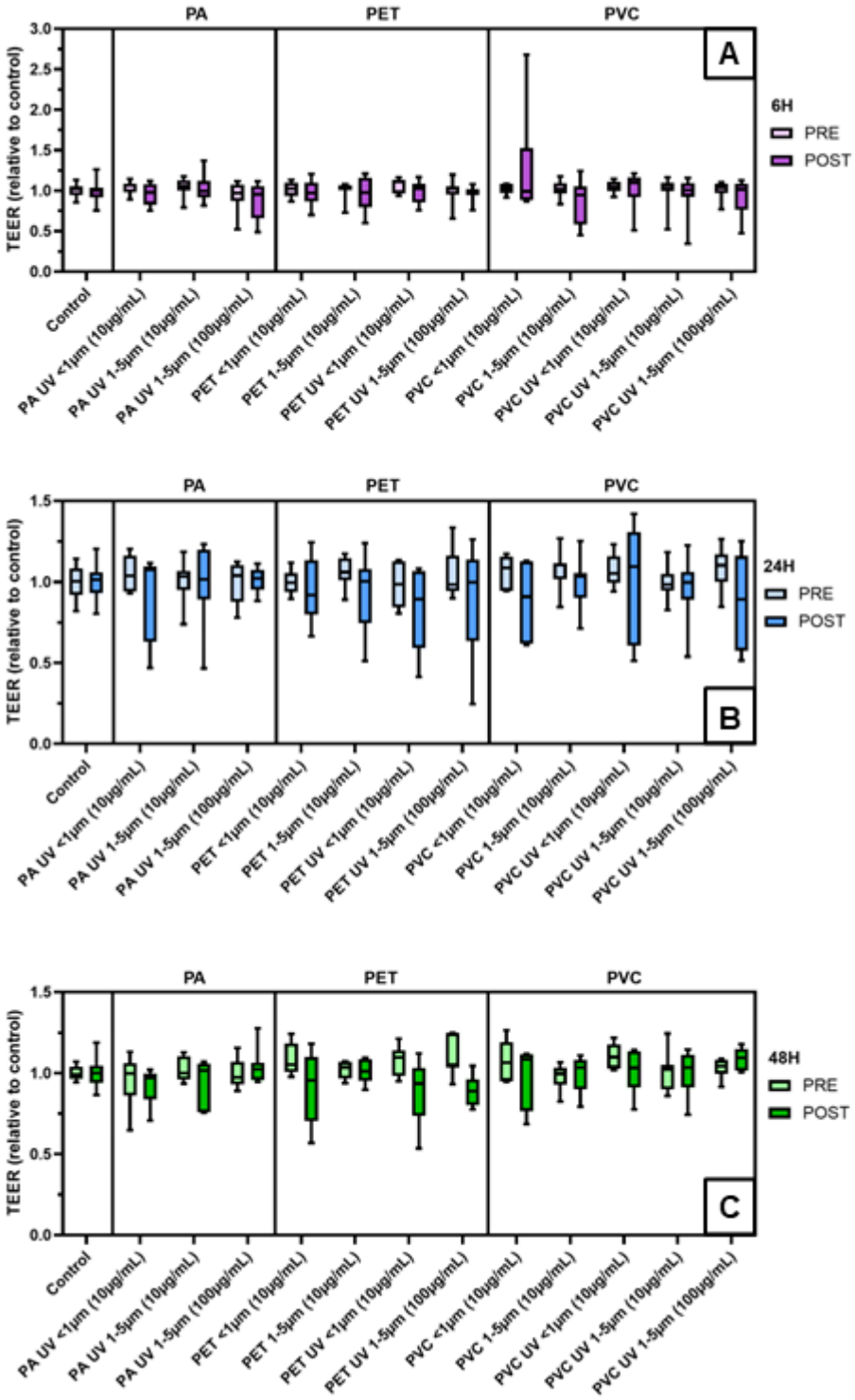

Figure S4 – **(A)** Box-and-whisker plots for TEER values after 6 hours, **(B)** box-and-whisker plots for TEER values after 24 hours and **(C)** box-and-whisker plots for TEER values after 48 hours of exposure. TEER values are shown relative to the control (set at 1.0), with data presented as median ± interquartile range. Co-cultures were exposed to PA, PET, or PVC particles, either virgin or UV-aged, in two size ranges (<1 µm and 1–5 µm) and at two concentrations (10 µg/mL and 100 µg/mL). Transepithelial electrical resistance (TEER) was assessed before (PRE) and after (POST) MNP exposure for three different exposure durations (6 h, 24 h and 48 h).